Acta Biotheor (2011) 59:291–312
DOI 10.1007/s10441-011-9137-x

REGULAR ARTICLE

Solvent Dielectric Effect and Side Chain Mutation on the Structural Stability of *Burkholderia cepacia* Lipase Active Site: A Quantum Mechanical/Molecular Mechanics Study

A. Tahan · M. Monajjemi

Received: 25 August 2009 / Accepted: 11 June 2011 / Published online: 28 June 2011

Abstract Quantum mechanical and molecular dynamics methods were used to analyze the structure and stability of neutral and zwitterionic configurations of the extracted active site sequence from a *Burkholderia cepacia* lipase, histidyl-seryl-glutamin (His86-Ser87-Gln88) and its mutated form, histidyl-cysteyl-glutamin (His86-Cys87-Gln88) in vacuum and different solvents. The effects of solvent dielectric constant, explicit and implicit water molecules and side chain mutation on the structure and stability of this sequence in both neutral and zwitterionic forms are represented. The quantum mechanics computations represent that the relative stability of zwitterionic and neutral configurations depends on the solvent structure and its dielectric constant. Therefore, in vacuum and the considered non-polar solvents, the neutral form of the interested sequences is more stable than the zwitterionic form, while their zwitterionic form is more stable than the neutral form in the aqueous solution and the investigated polar solvents in most cases. However, on the potential energy surfaces calculated, there is a barrier to proton transfer from the positively charged ammonium group to the negatively charged carboxylat group or from the ammonium group to the adjacent carbonyl oxygen and or from side chain oxygen and sulfur to negatively charged carboxylat group. Molecular dynamics simulations (MD) were also performed by using periodic boundary conditions for the zwitterionic configuration of the hydrated molecules in a box of water molecules. The obtained results demonstrated that the presence of explicit water molecules provides the more compact structures of the studied molecules. These simulations also indicated that side chain mutation and replacement of sulfur with oxygen leads to reduction of molecular flexibility and packing.

A. Tahan
Semnan Branch, Islamic Azad University, Semnan, Iran

M. Monajjemi (✉)
Department of Chemistry, Science and Research Branch, Islamic Azad University, Tehran, Iran
e-mail: m_monajjemi@yahoo.com

Keywords *Burkholderia cepacia* lipase · Solvent effect · Side chain mutation · Molecular dynamics simulation

1 Introduction

Lipases (EC 3.1.1.3) are important enzymes with a broad variety of industrial applications due to the multiplicity of reactions they catalyze. Due to their unique structural characteristics, lipases can catalyze reactions including organic substrates at the interface of organic and aqueous phases and can preserve their catalytic activity in organic solvents, biphasic systems and in micellar solutions (see Grochulski et al. 1993; Pugazhenthi and Kumar 2004; Han and Rhee 1986). The rising interest in lipase mainly lies in their efficiency in the syntheses of enantiomerically pure products. Synthesis of only one enantiomer, instead of racemic mixtures, is a necessity in pharmaceutical industry because often only one enantiomer has the desired activity, whereas no activity or even undesirable side effects reside in the other enantiomer.

Our QM/MM study concentrates on the lipase active site from *Burkholderia cepacia* (formerly *Pseudomonas cepacia*) because of the industrial importance of these enzymes and lack of quantum mechanics (QM) studies in this regard.

This lipase has an active site where the reaction is catalyzed by a catalytic triad (Ser87, Asp264, and His286). There is a large amount of experimental data available for *B. cepacia* lipase (BCL): The enantioselectivity and substrate specificity of the lipase from *P. cepacia* (Tuomi and Kazlauskas 1999; Tafi et al. 2000; Tomić and Kojić-Prodić 2002), kinetic measurements (Schmid and Verger 1998; Ljubovic and Sunjic 2000; Faber 1997), crystal structures of native enzyme and its complexes with the triglyceride like- and secondary alcohol ester like-inhibitors (Kim et al. 1997; Lang et al. 1998; Lui'c et al. 2001) and MD simulations (Tafi et al. 2004; Guieysse et al. 2003).

As we know, Hydration and mutation are important issues in molecular biophysics. The effect of hydration on the binding properties of proteins is still not fully understood. Often protein modeling is performed without explicit water molecules. On the other hand, the stability of proteins is partly determined by hydrophobic forces, which are mostly attributed to water. Proteins fold such that the polar side chains are exposed to the water and the hydrophobic side chains are closely packed inside. Hence, proteins in their native states are compact and not extended (Creighton 1993). The importance of water molecules in the active site of proteins have been clearly shown and presented in the literature where attempts have failed to model proteins, without taking into account water explicitly (Tajkhorshid et al. 1997).

Many of the current models treat solvation macroscopically. In particular it is not common to treat the structural and electronic effects of solvent molecules explicitly in quantum calculations (Jalkanen and Suhai 1996). In addition, many empirical force field calculations have not treated the effect of the solvent explicitly (Honig et al. 1993). Hence, we have investigated one of the BCL active site sequences, His86-Ser87-Gln88,and have studied the effect of solvation and side chain mutation of catalytic serine at a microscopic level on the structure and stability of zwitterionic and neutral configurations by using quantum mechanical and molecular dynamics

methods. This sequence can be considered as an example of a small model biomolecule with hydration phenomena analogous to the effect of solvation and side chain mutation on protein conformation.

In order to get realistic starting models for His-Ser-Gln sequence in vacuum and aqueous solution, His86-Ser87-Gln88 sequence of lipase enzyme was extracted. In addition, the active site Ser87 was replaced with Cys87 in both zwitterionic and neutral forms to investigate the effects of side chain mutation of catalytic serine on the molecular stability; structure and flexibility (see Fig. 1).

Molecular dynamics (MD) simulations were also performed using periodic boundary conditions for the zwitterionic form of His86-Ser87-Gln88 and His86-Cys87-Gln88 hydrated structures in a box of water molecules as described in Sect. 2.1, in order to study the effect of explicit water molecules and side chain mutation on the structure, its stability and its flexibility.

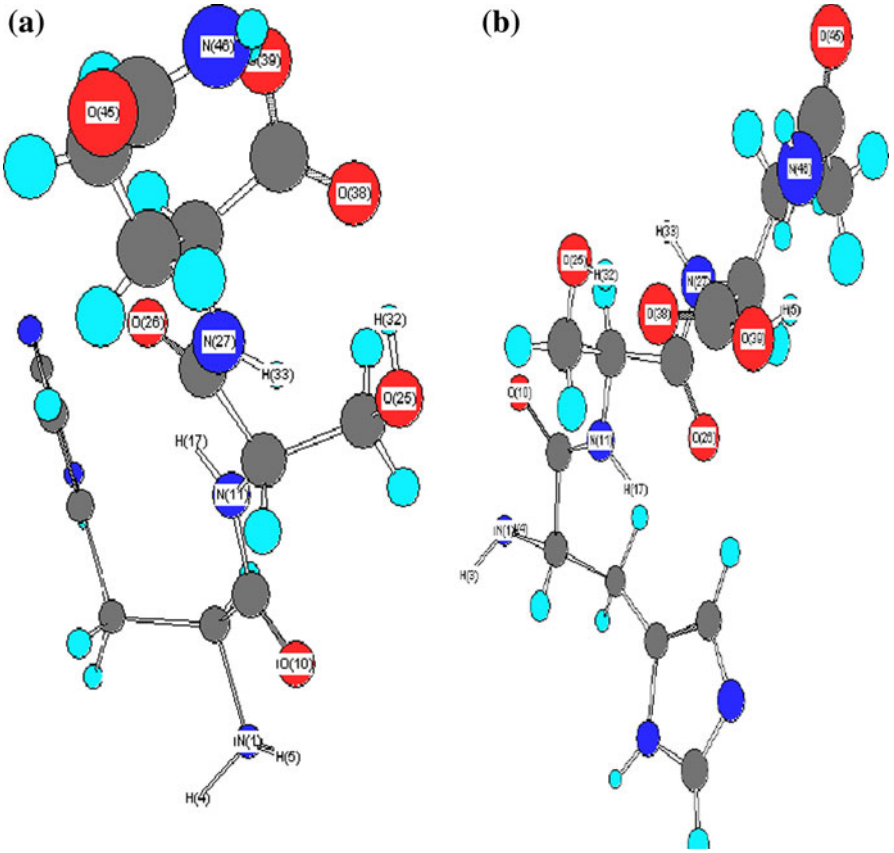

Fig. 1 The optimized structures of His-Ser-Gln (**a**) zwitterionic and (**b**) neutral sequence in B3LYP/6-31G* level of theory

Based on quantum mechanical studies and MD simulations, the aim of this work is to present quantitative answers to the following questions concerning the zwitterionic and neutral configurations of the interested compounds:

1. Which form, the zwitterionic or the neutral one, is more stable in vacuum, and polar or non-polar solutions?
2. What is the solvent dielectric constant effect on the relative stability and polarity of zwitterionic and neutral forms?
3. What is the effect of side chain mutation and replacement of sulfur with oxygen on the structural stability, molecular flexibility and polarity in both zwitterionic and neutral configurations?
4. What is role of explicit water molecules on the structural parameters of zwitterionic form in aqueous solution?
5. How can the resonance energy associated with donor–acceptor interactions in the zwitterionic and neutral structures of the interested compounds influence the relative stability of the corresponding sequences?
6. How can the donor–acceptor interactions influence the occupancies of the involved bonds, both in their zwitterionic and neutral structures?

2 Computational Details

2.1 Molecular Dynamics Simulations

The coordinate of utilized *B. cepacia* lipase (BCL) in this study was obtained from the crystal structure with entry number 3LIP in the Brookhaven Protein Data Bank. His86-Ser87-Gln88 sequence of the enzyme was then extracted from BCL, serine side chain was mutated, and His86-Cys87-Gln88 sequence was obtained by using Swiss Pdbviewer software (Guex and Peitsch 1997).

All calculations were done using the chemistry at Harvard molecular mechanics (CHARMM) program (Brooks et al. 1983) with the all atom 22 protein force field (MacKerell et al. 1998). Initial hydrogen positions were calculated using the HBUILD facility (Brünger and Karplus 1988) of the CHARMM program. The neutral state of the His residue were determined in all computations.

All molecular dynamics simulations were carried out with periodic boundary conditions.

The zwitterionic structure was solvated at the center of a 33A° × 33A° × 33A° cube of pre-equilibrated water molecules at $T = 300$ K and $p = 1$ atm. The water molecules for which the oxygen atoms were closer than 2.8 A° to any non-hydrogen peptide atom were removed. The resulting molecular systems contained 591 and 585 atoms for His-Ser-Gln and His-Cys-Gln sequences, respectively. The water molecules plus peptide system were minimized in CHARMM by performing 1,500 steps of steepest-descent (SD) minimization followed by 1,500 steps of adopted basis Newton–Raphson (ABNR) minimization (Jacoby et al. 1972; Wiberg 1965). The systems were gradually heated from 0 to 300 K in a 1,200 ps period. An equilibration

period of 1,200 ps followed, and molecular dynamics simulations of 40 ns at 300 K were performed.

After equilibration, the trajectory coordinates were recorded every 1 ps during a 40 ns simulation. Newton's equations were integrated using the leapfrog Verlet algorithm with a time step of 2 fs using the TIP3P (Jorgensen et al. 1983) water model, which is normal for simulations of solvated biomolecules when the hydrogens are constrained with a SHAKE algorithm (Berendsen et al. 1984), which is the case here. A non-bonded group based cut-off of 14Å was used, and the non-bonded pair list was updated every 100 steps. Standard analyses were performed on the calculated trajectories, which include time evolution of the root mean square deviation (RMSD) of coordinates with respect to the starting structure, to determine general stability, root-mean-squared fluctuations (RMSF) and the radius of gyration (*R*g). Hydrogen bonds and their life-times were calculated during the simulations using the criterion r (H-Acceptor) 2.4 A°. Diffusion coefficients were computed over the simulation time using the Einstein relation.

2.2 Molecular Modeling and DFT Calculations

Density functional theory (DFT) and molecular orbital (MO) calculations were carried out using MP2/3-21G*//B3LYP/3-21G*, B3LYP/6-311G*//B3LYP/6-31G* and B3LYP/6-31G*//B3LYP/6-31G* levels of theory with the GAUSSIAN 98 program package (Frisch et al. 1998). Energy minimum molecular geometries were located by minimizing energy, with respect to all geometrical coordinates without imposing any symmetrical constraints. Input structures for quantum mechanical calculations were obtained by molecular dynamics simulations utilizing CHARMM program. To model the bulk effects on zwitterionic and neutral configurations, the volume calculation was performed to determine cavity radii required for the use in the Onsager solvent model. The Onsager model as implemented in Gaussian 98 is a reaction field continuum model and is a method to predict the solvation effect on properties of the solute without considering explicit solvent molecules (Foresman and Frisch 1996; Tomasi and Persico 1994). Application of the Onsager continuum model requires a cavity radius and a dielectric constant.

Natural bond orbital (NBO) analysis was then performed on optimized structures in vacuum and different solvent media by using B3LYP/6-31G* level of theory by NBO 3.1 program (Glendening et al. 1988; Reed et al. 1988). The natural charges of heavy atoms, the antibonding and lone pair orbital occupancies in the optimized structures of compounds His-Ser-Gln and His-Cys-Gln, the stabilization energies associated with LP(1) $O_{10} \rightarrow \sigma^*_{N1–H5}$,LP(2) $O_{10} \rightarrow \sigma^*_{N1–H5}$, LP(1) $O_{38} \rightarrow \sigma^*_{o25–H32}$ LP(2) $O_{38} \rightarrow \sigma^*_{o25–H32}$, LP(1) $O_{38} \rightarrow \sigma^*_{S25–H32}$,LP(2) $O_{38} \rightarrow \sigma^*_{S25–H32}$ delocalizations for the zwitterionic structure and LP(1) $O_{10} \rightarrow \sigma^*_{o39–H5}$, LP(2) $O_{10} \rightarrow \sigma^*_{o39–H5}$, LP(1) $O_{2\ 6} \rightarrow \sigma^*_{o25–H32}$ LP(2) $O_{26} \rightarrow \sigma^*_{o25–H32}$, LP(1) $O_{26} \rightarrow \sigma^*_{S25–H32}$,LP(2) $O_{26} \rightarrow \sigma^*_{S25–H32}$ delocalizations for the neutral structure were calculated by using NBO analysis.

3 Results and Discussion

3.1 Quantum Mechanics Calculations

Ab initio molecular orbital (MO) and Beck's three parameter hybrid with the Lee–Yang–Parr correlation functional, B3LYP (Becke 1993; Lee et al. 1988), methods along with the 3-21G(d),6-31G(d),6-311G(d) basis sets were used for geometrical optimizations and single-point energy calculations of zwitterionic and neutral configurations of His-Ser-Gln and His-Cys-Gln sequences. The effects of solvent dielectric constant, explicit water molecules and side chain mutation on the structural parameters were investigated.

All methods used confirmed that in vacuum and the considered non-polar solvents (Carbon Tetrachloride and Diethyl Ether), the neutral configuration of the interested sequences is more stable than the zwitterionic configuration, while their zwitterionic configuration is more stable than the neutral configuration in the aqueous solution and the polar solvents (Dimethyl sulfoxide, DMSO, Ethanol and Tetrahydrofuran, THF,) in most cases (see Table 1). So, it can be concluded that on the potential energy surfaces studied, there is a barrier to proton transfer from (1) the positively charged ammonium group to the negatively charged carboxylat group. (2) The ammonium group to the adjacent carbonyl oxygen. (3) Side chain oxygen and sulfur to negatively charged carboxylat group.

The results also recall that the solvent bulk considerably stabilizes zwitterionic form rather than vacuum. In addition, energy variance between neutral and zwitterionic forms in vacuum is more than it is in different solvent media. Therefore, in most cases, increase in energy variance between neutral and zwitterionic forms results from increase in solvent dielectric constant.

On the other hand, our findings demonstrate that the energy variance between neutral and zwitterionic configurations of His-Ser-Gln sequence is more than it is for His-Cys-Gln in water bulk while it is less in vacuum. Moreover, the side chain mutation doesn't have the regular effect on the energy variance in different solvent media (His-Ser-Gln vs. His-Cys-Gln values).However, it mainly depends on the solvent structure.

The comparison of structural parameters represent that their values are different in vacuum and different solvent media while they are very similar in water and polar solvents (see Table 2).

A useful aspect of NBO method is that it gives information about interactions in both filled and virtual spaces that could enhance the analysis of intra-and intermolecular interactions. The second order Fock matrix was carried out to evaluate the donor–acceptor interactions in the NBO basis. The interactions result in a loss of occupancy from the localized NBO of the idealized Lewis structure into an empty non-Lewis orbital. For each donor (i) and acceptor (j), the stabilization energy E (2) associated with the delocalization $i \rightarrow j$ is estimated as:

$$E(2) = \Delta E_{ij} = q_i \frac{F(i,j)^2}{\varepsilon_j - \varepsilon_i} \quad (1)$$

Where q_i is the donor orbital occupancy, ε_i and ε_j are diagonal elements and F (i, j) is the off diagonal NBO Fock matrix element.

Table 1 Calculated relative energy values (ΔE_{el} in kcal mol^{-1}) and dipole moments (μ in Debye) for the zwitterionic (Z) and neutral (N) configurations of His-Ser-Gln (1a and 1b compounds) and His-Cys-Gln (2a and 2b compounds) sequences in different levels of theory and solvent dielectric constants (ε)

		MP2/3-21G*//B3LYP/3-21G*		B3LYP/6- 311G*//B3LYP/6-31G*		B3LYP/6- 31G*//B3LYP/6-31G*		μ	$\Delta\mu$
Compounds	ε^*	E_{el}	ΔE_{el}	E_{el}	ΔE_{el}	E_{el}	ΔE_{el}		
1a-His-Ser-Gln (Z)	1	−1,314.1028	0.00	−1,326.9070	36.48	−1,326.5660	37.44	33.1358	23.5427
1b-His-Ser-Gln (N)	1	−1,314.1028	0.00	−1,326.9651	0.00	−1,326.6257	0.00	9.5931	
1a-His-Ser-Gln (Z)	2.22	−1,314.1450	43.11	−1,326.9494	16.69	−1,326.6068	19.27	41.1746	23.3237
1b-His-Ser-Gln (N)	2.22	−1,314.1715	0.00	−1,326.9760	0.00	−1,326.6375	0.00	17.8509	
1a-His-Ser-Gln (Z)	4.33	−1,314.1752	1.01	−1,326.9802	0.87	−1,326.6370	3.73	46.3309	26.9285
1b-His-Ser-Gln (N)	4.33	−1,314.1768	0.00	−1,326.9816	0.00	−1,326.6429	0.00	19.4024	
1a-His-Ser-Gln (Z)	7.58	−1,314.1935	0.00	−1,326.9995	0.00	−1,326.6558	0.00	49.4969	29.2057
1b-His-Ser-Gln (N)	7.58	−1,314.1800	8.48	−1,326.9850	9.12	−1,326.6462	6.02	20.2912	
1a-His-Ser-Gln (Z)	24.55	−1,314.2146	0.00	−1,327.0219	0.00	−1,326.6775	0.00	53.2353	32.0065
1b-His-Ser-Gln (N)	24.55	−1,314.1834	19.54	−1,326.9887	20.88	−1,326.6497	17.43	21.2288	
1a-His-Ser-Gln (Z)	46.7	−1,314.2196	0.00	−1,327.0274	0.00	−1,326.6828	0.00	54.1764	32.7214
1b-His-Ser-Gln (N)	46.7	−1,314.1594	37.81	−1,326.9895	23.78	−1,326.6506	20.25	21.4550	
1a-His-Ser-Gln (Z)	78.39	−1,314.2220	0.00	−1,327.0299	0.00	−1,326.6853	0.00	54.6291	33.0794
1b-His-Ser-Gln (N)	78.39	−1,314.1846	23.44	−1,326.9899	25.09	−1,326.6510	21.57	21.5497	
2a-His-Cys-Gln (Z)	1	−1,635.3243	45.32	−1,649.8761	40.64	−1,649.5317	41.33	33.8082	23.8026
2b-His-Cys-Gln (N)	1	−1,635.3965	0.00	−1,649.9409	0.00	−1,649.5976	0.00	10.0056	
2a-His-Cys-Gln (Z)	2.22	−1,635.3677	23.33	−1,649.9119	19.77	−1,649.5665	20.14	40.6237	0.8104
2b-His-Cys-Gln (N)	2.22	−1,635.4049	0.00	−1,649.9505	0.00	−1,649.6081	0.00	41.4341	
2a-His-Cys-Gln (Z)	4.33	−1,635.4002	6.36	−1,649.9518	2.07	−1,649.6053	4.63	47.4575	28.4552
2b-His-Cys-Gln (N)	4.33	−1,635.4103	0.00	−1,649.9551	0.00	−1,649.6127	0.00	19.0023	
2a-His-Cys-Gln (Z)	7.58	−1,635.4202	0.00	−1,649.9529	3.11	−1,649.6063	5.67	47.6307	27.8672
2b-His-Cys-Gln (N)	7.58	−1,635.4136	4.19	−1,649.9578	0.00	−1,649.6153	0.00	19.7635	

Table 1 continued

Compounds	ε^*	MP2/3-21G*//B3LYP/3-21G*		B3LYP/6- 311G*//B3LYP/6-31G*		B3LYP/6- 31G*//B3LYP/6-31G*		μ	$\Delta\mu$
		E_{el}	ΔE_{el}	E_{el}	ΔE_{el}	E_{el}	ΔE_{el}		
2a-His-Cys-Gln (Z)	24.55	−1,635.4430	0.00	−1,649.9693	0.00	−1,649.6483	0.00	55.2428	34.6872
2b-His-Cys-Gln (N)	24.55	−1,635.4170	16.35	−1,649.9607	5.40	−1,649.6182	18.94	20.5556	
2a-His-Cys-Gln (Z)	46.7	−1,635.4486	0.00	−1,649.9614	7.831	−1,649.6541	0.00	56.3459	35.6090
2b-His-Cys-Gln (N)	46.7	−1,635.4178	19.32	−1,649.9739	0.00	−1,649.6188	22.13	20.7369	
2a-His-Cys-Gln (Z)	78.39	−1,635.4511	0.00	−1,649.9766	0.00	−1,649.6293	0.00	51.7014	30.8811
2b-His-cys-Gln (N)	78.39	−1,635.4181	20.71	−1,649.9617	9.31	−1,649.6191	6.39	20.8203	

* The mentioned values are dielectric constant for vacuum, carbon tetrachloride, diethyl ether, tetrahydrofuran, ethanol, dimethyl sulfoxide and water media, respectively

Table 2 The calculated structural parameters (Bond length R; Bond angle Θ; and Dihedral angle φ) for involved bonds and angles in the optimized zwitterionic (a) and neutral (b) structures of His-Ser-Gln (1a and 1b) and His-Cys-Gln (2a and 2b) compounds using QM methods based on B3LYP/6-31G* level of theory in different solvent media and MD simulations in water box using CHARMM force field

Compound	1a 1b	2a 2b	1a 1b	2a 2b	1a 1b	2a 2b	1a 1b	2a 2b	1a 1b	2a 2b	1a 1b	2a 2b	1a 1b	2a 2b	2a RMSF (A°)	1a
ε	1	1	2.22	2.22	4.33	4.33	7.58	7.58	24.55	24.55	46.7	46.7	78.39	78.39	Water box	Water box
Bond length (R)																
(A°)																
R_{1-2}	1.514	1.516	1.521	1.521	1.524	1.524	1.525	1.524	1.527	1.527	1.527	1.528	1.527	1.526	1.494	1.491
	1.47	1.471	1.464	1.465	1.463	1.464	1.462	1.463	1.462	1.462	1.461	1.462	1.461	1.462		
R_{1-5}	1.117	1.102	1.068	1.071	1.054	1.053	1.048	1.052	1.042	1.041	1.041	1.040	1.041	1.046	1.040	1.040
	–	–	–	–	–	–	–	–	–	–	–	–	–	–		
R_{5-39}	–	–	–	–	–	–	–	–	–	–	–	–	–	–	–	–
	0.981	0.981	0.983	0.982	0.984	0.983	0.985	0.984	0.986	0.985	0.987	0.985	0.987	0.985		
R_{2-7}	1.564	1.565	1.565	1.565	1.565	1.565	1.565	1.565	1.567	1.566	1.567	1.567	1.567	1.566	1.543	1.573
	1.542	1.543	1.540	1.539	1.541	1.540	1.541	1.541	1.542	1.541	1.542	1.541	1.542	1.542		
R_{7-10}	1.256	1.253	1.243	1.244	1.238	1.238	1.235	1.238	1.232	1.232	1.232	1.232	1.231	1.235	1.240	1.225
	1.232	1.231	1.233	1.498	1.233	1.232	1.234	1.232	1.235	1.233	1.235	1.233	1.235	1.233		
R_{7-11}	1.311	1.313	1.329	1.326	1.340	1.341	1.348	1.341	1.357	1.359	1.359	1.361	1.360	1.350	1.380	1.325
	1.362	1.363	1.365	1.366	1.366	1.367	1.366	1.367	1.366	1.367	1.366	1.368	1.366	1.367		
R_{11-16}	1.464	1.470	1.465	1.470	1.465	1.471	1.466	1.471	1.467	1.472	1.467	1.472	1.467	1.472	1.459	1.45
	1.460	1.467	1.463	1.471	1.462	1.471	1.462	1.470	1.461	1.470	1.461	1.469	1.461	1.469		
R_{16-20}	1.565	1.552	1.563	1.553	1.563	1.555	1.564	1.555	1.564	1.557	1.565	1.557	1.565	1.556	1.547	1.591
	1.548	1.543	1.548	1.543	1.548	1.543	1.548	1.543	1.549	1.544	1.549	1.544	1.549	1.544		
R_{16-21}	1.540	1.551	1.538	1.550	1.539	1.550	1.540	1.551	1.543	1.554	1.544	1.555	1.545	1.552	1.507	1.550
	1.535	1.541	1.535	1.542	1.535	1.541	1.534	1.541	1.534	1.541	1.534	1.541	1.534	1.541		

Table 2 continued

Compound	1a 1b	2a 2b	1a 1b	2a 2b	1a 1b	2a 2b	1a 1b	2a 2b	1a 1b	2a 2b	1a 1b	2a 2b	1a 1b	2a 2b	2a RMSF (A°)	1a
ε	1	1	2.22	2.22	4.33	4.33	7.58	7.58	24.55	24.55	46.7	46.7	78.39	78.39	Water box	Water box
$R_{20–25}$	1.395	1.835	1.404	1.837	1.411	1.84	1.416	1.840	1.422	1.844	1.423	1.845	1.424	1.842	1.425	1.804
	1.403	1.838	1.404	1.838	1.405	1.838	1.406	1.839	1.407	1.839	1.407	1.839	1.407	1.838		
$R_{21–26}$	1.240	1.244	1.233	1.237	1.229	1.231	1.227	1.231	1.224	1.225	1.224	1.225	1.224	1.228	1.220	1.207
	1.233	1.227	1.233	1.227	1.235	1.228	1.235	1.229	1.236	1.230	1.236	1.230	1.236	1.230		
$R_{21–27}$	1.341	1.327	1.355	1.341	1.367	1.358	1.375	1.358	1.385	1.378	1.388	1.381	1.389	1.369	1.342	1.319
	1.355	1.359	1.355	1.358	1.355	1.359	1.355	1.359	1.355	1.359	1.355	1.359	1.355	1.359		
$R_{27–31}$	1.472	1.469	1.467	1.467	1.465	1.467	1.463	1.467	1.462	1.465	1.462	1.465	1.462	1.462	1.428	1.461
	1.457	1.457	1.459	1.459	1.458	1.458	1.458	1.458	1.458	1.458	1.458	1.458	1.458	1.458		
$R_{31–35}$	1.575	1.576	1.572	1.570	1.570	1.564	1.568	1.564	1.567	1.558	1.567	1.557	1.566	1.572	1.540	1.535
	1.549	1.549	1.547	1.547	1.547	1.547	1.547	1.547	1.547	1.547	1.547	1.547	1.548	1.547		
Bond Angle (Θ)																
(°)																
$\Theta_{1–6}$	112.1	112.4	111.4	111.6	111.0	111.0	110.8	110.0	110.5	110.3	110.4	110.2	110.3	110.6	109.9	113.8
	116.7	116.6	116.7	116.2	116.0	116.6	117.2	116.8	117.5	117.0	117.5	117.1	117.6	117.2		
$\Theta_{1–7}$	100.8	100.8	102.2	102.0	103.1	103.2	103.7	103.3	104.5	104.7	104.7	104.0	104.8	104.0	114.4	110.9
	108.1	108.3	106.5	105.9	106.6	106.0	106.7	106.1	106.7	106.2	106.8	106.3	106.7	106.3		
$\Theta_{2–11}$	118.8	118.7	118.6	118.6	118.8	118.0	118.9	118.0	119.1	119.4	119.1	119.4	119.1	119.2	119.0	121.3
	114.3	114.2	115.4	115.7	115.1	115.3	114.9	115.0	114.7	114.8	114.6	114.8	114.6	114.7		
$\Theta_{2–9}$	114.3	114.0	113.0	114.0	113.9	113.9	113.8	113.9	113.8	113.8	113.8	113.9	113.8	113.9	117.1	117.7
	114.3	114.3	113.2	113.5	112.9	113.2	112.7	112.0	112.6	112.8	112.5	112.8	112.5	112.7		

Table 2 continued

Compound	1a 1b	2a 2b	1a 1b	2a 2b	1a 1b	2a 2b	1a 1b	2a 2b	1a 1b	2a 2b	1a 1b	2a 2b	1a 1b	2a 2b	2a RMSF (A°)	1a
ε	1	1	2.22	2.22	4.33	4.33	7.58	7.58	24.55	24.55	46.7	46.7	78.39	78.39	Water box	Water box
Θ_{7-16}	125.2	124.6	122.7	122.0	121.6	121.5	121.1	121.5	120.6	120.4	120.5	120.2	120.4	120.8	119.1	122.4
	121.9	121.0	121.3	121.4	121.4	121.5	121.5	121.7	121.6	121.8	121.6	121.8	121.7	121.8		
Θ_{11-21}	104.5	103.4	107.1	105.1	108.9	107.1	110.1	107.2	111.5	109.6	111.8	109.9	111.0	108.4	110.5	114.8
	114.9	113.4	114.4	112.0	114.4	112.9	114.4	114.4	114.4	112.9	114.4	112.9	114.4	112.9		
Θ_{11-20}	111.8	110.8	111.6	110.2	111.1	109.6	110.8	109.5	110.3	108.8	110.2	108.6	110.2	109.2	110.1	112.7
	110.9	108.0	111.1	108.0	111.1	108.9	111.2	108.8	111.2	108.8	111.2	108.8	111.2	108.8		
Θ_{16-27}	114.9	115.8	114.1	115.8	113.7	115.8	113.5	115.8	113.4	115.9	113.4	115.9	113.4	115.9	115.7	115.8
	117.7	116.8	117.9	116.8	118.2	117.0	118.4	117.2	118.5	117.3	118.5	117.3	118.5	117.3		
Θ_{16-25}	111.0	115.5	111.5	115.9	112.1	116.2	112.4	116.3	112.8	116.7	112.8	116.8	112.9	116.5	113.1	112.3
	115.5	114.4	111.4	114.4	111.3	114.4	111.3	114.4	111.3	114.4	111.3	114.4	111.3	114.4		
Θ_{20-21}	110.6	112.1	110.5	112.3	110.5	112.5	110.5	112.5	110.6	112.7	110.6	112.7	110.6	112.5	114.2	109.6
	109.2	110.6	109.3	110.7	109.3	110.7	109.3	110.7	109.3	110.8	109.3	110.8	109.4	110.8		
Θ_{21-31}	121.4	124.9	122.3	124.1	122.4	123.5	122.3	123.5	122.2	123.1	122.2	123.1	122.2	123.3	126.4	122.6
	123.1	122.3	122.7	122.2	122.1	121.8	121.7	121.5	121.4	121.3	121.4	121.2	121.3	121.2		
Θ_{27-35}	110.2	105.7	110.7	107.3	111.3	109.4	111.7	109.5	112.3	112.2	112.4	112.7	112.5	110.7	109.7	108.8
	112.5	113.3	112.3	113.1	112.3	113.1	112.2	113.0	112.2	113.0	112.2	113.0	112.2	113.0		
Dihedral (φ) (°)																
φ_{1-9}	−154.5	−153.5	154.4	−154.7	−154.9	−155.1	−155.1	−155.1	−155.1	−154.8	−155	−154.8	−154	−154	−170.6	−173.4
	−152.8	−149.7	−169.5	−171.6	−168.7	−170.8	−167.9	−169.9	−167.2	−169.1	−166.8	−168.9	−168.8	−168.2	9.095	7.808
φ_{1-11}	−176.6	−170.3	−177.5	−176.1	−178.7	−177	−178.5	−177.9	−178.5	−178.7	−178.5	−178.7	−178.5	−178.8	140.7	156.4
	40.6	37.7	76.2	83.5	73.4	79.0	71.2	77.3	69.1	75.3	68.2	74.8	68.3	73.4	25.789	18.119

Table 2 continued

Compound	1a 1b	2a 2b	1a 1b	2a 2b	1a 1b	2a 2b	1a 1b	2a 2b	1a 1b	2a 2b	1a 1b	2a 2b	1a 1b	2a 2b	2a RMSF (A°)	1a
ε	1	1	2.22	2.22	4.33	4.33	7.58	7.58	24.55	24.55	46.7	46.7	78.39	78.39	Water box	Water box
φ_{2-16}	178.4	174.0	178.8	−179.7	−179.2	−176.9	−177.5	−176.8	−175.4	−173.9	−174.9	−173.4	−174.7	−175.4	−177.4	−179.7
	−167	−168.1	−165.4	−163	−165.6	−163	−165.9	−163.3	−166.3	−163.6	−166.5	−163.7	−166.5	−164.1	7.159	6.634
φ_{6-11}	−55.5	−48.3	−56.1	−54.4	−56.9	−55.0	−56.4	−55.9	−55.0	−56.1	−55.9	−55.0	−55.9	−56.5	−94.6	−80.9
	169.9	166.9	−156.3	−149.9	−158.4	−152.8	−160.2	−155	−161.8	−156.7	−162.6	−157.1	−162.5	−158.3	12.566	18.179
φ_{6-18}	178.6	179.1	179.4	179.2	179.7	179.6	180.0	179.6	−179.7	180.0	−180	180.0	−180	179.7	−179.1	−179.8
	−178.3	−178.3	−176.4	−176.7	−176	−176.2	−175.7	175.0	−175.4	−175.7	−175.3	−175.6	−175.3	−175.5	6.354	6.137
φ_{6-19}	−178.8	−179.5	−180.0	−179.7	179.7	180.0	179.4	180.0	179.2	179.4	179.2	179.4	179.2	179.7	178.9	179.9
	177.7	177.7	175.6	175.9	175.1	175.4	174.8	−175.9	174.4	174.8	174.3	174.7	174.3	174.6	6.844	6.683
φ_{7-9}	90.7	90.8	89.3	88.8	87.7	87.1	86.6	87.0	85.6	85.4	85.4	85.2	85.3	86.3	65.1	62
	82.6	85.6	68.7	67.8	69.0	68.1	69.4	68.5	69.8	68.9	70.0	69.0	69.0	69.5	9.25	7.798
φ_{7-20}	80.9	88.7	82.1	78.1	80.9	74.0	80.3	74.9	79.8	73.2	79.6	73.1	79.5	73.6	149.3	154.9
	164.2	170.9	162.7	169.7	163.6	170.3	164.2	170.7	164.7	171.1	164.9	171.2	164.9	171.3	20.651	16.01
φ_{7-21}	−159.5	−151.1	−156.9	−160.7	−157.2	−162.8	−157.2	−162.8	−157	−163.2	−157	−163.1	−157	−157	−87.8	−80.8
	−72.2	−65.5	−72.9	−66.9	−71.0	−66.3	−71.4	−65.9	−70.9	−65.5	−70.7	−65.4	−70.7	−65.3	20.826	16.202
φ_{10-17}	−174.6	−173.9	−175.5	−177.2	−176.4	−178.4	−177.3	−178.4	−178.5	−180	−178.8	179.7	−178.9	−179.2	178.8	178.3
	168.2	167.8	166.5	166.5	179.3	165.7	165.3	165.1	164.8	164.7	164.6	164.6	164.6	164.3	7.550	7.68
φ_{11-25}	−178.8	−160	−174.1	−160.4	−173.4	−161.8	−173.4	−161.8	−173.8	−164.8	−173.9	−165.3	−174	−163.1	−96.2	−54.9
	−165.9	−161.5	−167.9	−163.1	−168.5	−163.9	−168.7	−164.3	−169.0	−164.7	−169.1	−164.8	−169.1	−164.8	51.529	57.641
φ_{11-27}	171.6	164.8	170.7	167.4	170.9	168.4	171.3	168.4	171.7	168.7	171.8	168.8	171.8	171.8	−152.892	168.9
	−1.6	−17.4	−2.0	103.9	−3.4	−18.6	−3.5	−18.5	−3.4	−18.4	−3.3	−18.4	−3.3	−18.2	72.794	29.162
φ_{16-31}	150.7	158.5	154.6	160.0	156.4	162.5	157.5	162.5	158.7	166.3	159.0	166.9	159.2	164.2	−179.7	−180
	169.1	174.6	165.8	172.7	164.7	171.7	164.0	170.0	163.3	170.3	162.0	170.2	162.0	169.9	7.810	7.356

Table 2 continued

Compound	1a 1b	2a 2b	1a 1b	2a 2b	1a 1b	2a 2b	1a 1b	2a 2b	1a 1b	2a 2b	1a 1b	2a 2b	1a 1b	2a 2b	2a RMSF (A°)	1a
ε	1	1	2.22	2.22	4.33	4.33	7.58	7.58	24.55	24.55	46.7	46.7	78.39	78.39	Water box	Water box
φ_{20-27}	−67.9	−75.8	−67.6	−72.8	−66.8	−71.2	−66.1	−71.2	−65.2	−70.1	−64.0	−69.8	−64.9	−70.8	−28.1	−66.4
	123.8	105.4	109.3	103.9	121.0	103.8	121.9	103.9	122.0	103.9	122.1	103.0	122.1	104.1	73.757	29.04
φ_{21-25}	−121.4	85.1	66.9	82.9	65.6	79.2	64.3	79.1	62.5	73.5	61.9	72.6	61.7	76.5	139.0	−112.7
	65.9	73.3	64.9	72.1	64.3	71.4	64.0	71.0	63.7	70.6	63.6	70.5	63.6	70.5	50.7	56.9
φ_{21-34}	155.8	102.0	139.1	105.7	134.8	110.2	132.4	110.3	130.4	114.0	130.1	114.3	130.0	130.0	144.1	140.0
	150.8	160.1	164.7	168.6	168.6	172.2	170.8	174.3	172.8	176.0	173.4	176.4	173.5	176.0	19.046	20.395
φ_{21-35}	−78.5	−132.6	−95.7	−130.2	−100.3	−126.8	−102.8	−126.8	−104.9	−124.8	−105.2	−124.8	−105.4	−126.5	93.6	97.7
	−84.5	−75.6	−71.2	−67.3	−67.2	−63.7	−64.0	−61.5	−63.0	−59.8	−62.4	−59.4	−62.3	−58.8	19.303	20.719
φ_{26-33}	−168.5	−168.4	−167.2	−169.1	−166.3	−169.2	−165.6	−169.2	−164.6	−169.2	−164.3	−169.2	−164.2	−169.3	−179.9	179
	157.7	178.7	178.2	−178.4	179.3	−177.7	179.7	−177.4	−179.6	−177.1	−179.3	−176	−179.4	−177.1	7.914	7.585
φ_{27-37}	−175.3	−171.7	−166.3	−171.4	−165.9	−171.7	−165.5	−171.7	−164.9	−171.9	−164.7	−172	−164.6	−171.7	−109.1	−145.8
	−168.7	−168.9	−178.4	179.1	177.6	−178.7	177.4	177.0	176.6	177.4	176.4	177.2	176.3	176.9	55.815	47.681

The performed NBO analyses demonstrate that the zwitterionic structure has the strong resonance energies for LP (1) $O_{10} \rightarrow \sigma^*_{N1–H5}$, LP (2) $O_{10} \rightarrow \sigma^*_{N1–H5}$, LP(1) $O_{38} \rightarrow \sigma^*_{o25–H32}$, LP(2) $O_{38} \rightarrow \sigma^*_{o25–H32}$, LP(1) $O_{38} \rightarrow \sigma^*_{S25–H32}$ and LP(2) $O_{38} \rightarrow \sigma^*_{S25–H32}$ delocalizations. These strong hydrogen bonds indicate that there is a proton transfer from the positively charged ammonium group to the adjacent carbonyl oxygen and from side chain oxygen and sulfur to negatively charged carboxylat group. Hence, the zwitterionic structure stabilizes in vacuum and the considered non-polar solvents. These results also show that by increasing the solvent dielectric constant, the mentioned resonance energies, $N_1–H_5$ bond length and $\sigma^*_{N1–H5}$,$\sigma^*_{o25–H32}$ and $\sigma^*_{S25–H32}$ antibonding pair orbitals occupancies decrease while LP O_{10} lone pair orbital occupancy increases.

The neutral structure also has the strong resonance energies for LP (1) $O_{10} \rightarrow \sigma^*_{O39–H5}$ and LP (2) $O_{10} \rightarrow \sigma^*_{O39–H5}$ delocalizations (see Table 3).our findings show that by increasing of solvent dielectric constant, the investigated resonance energies, $O_{39}–H_5$ bond length and $\sigma^*_{O39–H5}$ antibonding pair orbital occupancy increase. However, in neutral structure, a proton transfer is from the carboxylic group to the adjacent carbonyl oxygen and the neutral structure stabilizes in water and the considered polar solvents.

Therefore, it can be concluded that the energy variance and relative stability of zwitterionic and neutral structures are controlled by LP $O_{10} \rightarrow \sigma^*_{O39–H5}$ resonance energies.

The dipole moment is the first derivative of the energy with respect to the applied electric field. It is a measure of the asymmetry in the molecular charge distribution. Dipole moment of neutral and zwitterionic configurations of His-Ser-Gln and His-Cys-Gln sequences are reported in Table 1 at B3LYP/6-31G* level of theory. The obtained results reveal that the zwitterionic form of interested sequences has a higher dipole moment than the neutral form in all of the tested media. This fact reveals that the charge distribution in the neutral form is more symmetric than it is in the zwitterionic form in the interested level of theory. The table of data also demonstrates that by increasing of solvent dielectric constant, the dipole moment of the studied sequences increases. Hence, the highest dipole moment is perceived in aqueous solutions.

On the other hand, these results show that the side chain mutation doesn't have the regular effect on the dipole moment in different solvents (His-Ser-Gln vs. His-Cys-Gln values). However, it is mainly depended on the solvent structure.

3.2 Molecular Dynamics Simulations

Here, we present the results of MD simulations for the zwitterionic form of both His-Ser-Gln and His-Cys-Gln sequences, focusing on the obtained data in a long-term trajectory of 40 ns at T = 300 K generated as described in Sect. 2.1. Overall, the studied structures remain stable. The obtained results from time series analysis show that the RMSD and Rg average values for His-Cys-Gln are higher than those for His-Ser-Gln (2.616489 and 4.384516 Å vs. 2.434384 and 4.106820 Å), while the RMSD and Rg rms fluctuations for His-Cys-Gln are lower than those for

Table 3 Calculated lone pair (LP(1) and LP(2)) occupancies and antibonding orbital (σ^*) occupancies and resonance energies (LP → σ^*, in kcal mol^{-1}), for involved atoms and bonds in His-Ser-Gln (1a and 1b) and His-Cys-Gln (2a and 2b) compounds using natural bond orbital (NBO) analysis based on the optimized structures in B3LYP/6-31G* level of theory

Compound	1a	2a	1a	2a	1a	2a	1a	2a	1a	2a	1a	2a	1a
	1b	2b	1b	2b	1b	2b	1b	2b	1b	2b	1b	2b	1b
ε	1	1	2.22	2.22	4.33	4.33	7.58	7.58	24.55	24.55	46.7	46.7	78.39
Occupancies													
LP(1) O_{10}	1.96237	1.96321	1.96596	1.96568	1.96811	1.96838	1.96944	1.96845	1.97088	1.97122	1.97123	1.97159	1.97139
	1.96187	1.96096	1.95966	1.95953	1.95796	1.95792	1.95701	1.95696	1.95599	1.95605	1.95572	1.95584	1.95563
LP(2) O_{10}	1.78446	1.79475	1.82121	1.81970	1.83434	1.83735	1.84074	1.83775	1.84651	1.85049	1.84773	1.85181	1.84830
	1.87099	1.86970	1.87231	1.87097	1.87309	1.87180	1.874	1.87227	1.87384	1.87265	1.87441	1.87223	1.87443
LP(1) N_{11}	–	1.57668	1.62042	1.61342	1.64703	1.64610	1.66162	1.64688	1.67742	1.67792	1.68127	1.68192	1.68309
	1.69618	1.69971	1.70572	1.71116	1.70719	1.71311	1.70747	1.71399	1.70794	1.71470	1.70765	1.71500	1.70777
LP(1) O_{25}	1.97475	–	1.97702	–	1.97882	–	1.97977	–	1.98078	–	1.98101	–	1.98112
	1.97607	–	1.97619	–	1.97646	–	1.97654	–	1.97680	–	1.97677	–	1.97679
LP(2) O_{25}	1.91517	–	1.92347	–	1.92738	–	1.92892	–	1.93020	–	1.93048	–	1.93063
	1.94874	–	1.94915	–	1.94999	–	1.95032	–	1.95102	–	1.95098	–	1.95103
LP(1) S_{25}	–	1.98856	–	1.98983	–	1.99106	–	1.99109	–	1.99218	–	1.99230	–
	–	1.98972	–	1.98977	–	1.98984	–	1.98988	–	1.98993	–	1.98994	–
LP(2) S_{25}	–	1.95041	–	1.95182	–	1.95209	–	1.95210	–	1.95081	–	1.95042	–
	–	1.96660	–	1.96659	–	1.96721	–	1.96757	–	1.96795	–	1.96805	–
LP(1) N_{27}	1.62967	1.59554	1.68765	1.65214	1.70718	1.68359	1.71868	1.68431	1.73136	1.71295	1.73439	1.71650	1.73580
	1.68900	1.69617	1.68986	1.69596	1.69039	1.69613	1.69069	1.69624	1.69117	1.69630	1.69122	1.69644	1.69120
LP(1) O_{38}	1.94531	1.95673	1.94950	1.96160	1.95474	1.96723	1.95800	1.96740	1.96171	1.97332	1.96261	1.97397	1.96306
	1.97660	1.97657	1.97707	1.97695	1.97718	1.97702	1.97714	1.97706	1.97725	1.97708	1.97719	1.97715	1.85266
LP(2) O_{38}	1.84510	1.84724	1.85536	1.85814	1.85992	1.86614	1.86221	1.86630	1.86417	1.87188	1.86459	1.87241	1.86479
	1.84398	1.84496	1.84557	1.84638	1.84825	1.84858	1.85053	1.84976	1.85143	1.85104	1.85250	1.85062	1.85266

Table 3 continued

Compound	1a	2a	1a	2a	1a	2a	1a	2a	1a	2a	1a	2a	1a
	1b	2b	1b	2b	1b	2b	1b	2b	1b	2b	1b	2b	1b
ε	1	1	2.22	2.22	4.33	4.33	7.58	7.58	24.55	24.55	46.7	46.7	78.39
LP(3) O_{38}	1.61908	1.60035	–	–	–	–	–	–	–	–	–	–	–
	–	–	–	–	–	–	–	–	–	–	–	–	–
LP(1) O_{39}	1.95861	1.95746	1.95056	1.95310	1.94571	1.94842	1.94229	1.94830	1.93794	1.94460	1.93675	1.94464	1.93616
	1.96947	1.96899	1.96976	1.96919	1.96933	1.96881	1.96880	1.96859	1.96880	1.96836	1.96845	1.96857	1.96842
LP(2) O_{39}	1.87099	1.87198	1.88119	1.88239	1.88906	1.89233	1.89313	1.89255	1.89746	1.89766	1.89848	1.89718	1.89890
	1.79487	1.85878	1.79793	1.79882	1.79493	1.79649	1.79280	1.79522	1.79133	1.79377	1.79044	1.79389	1.79021
LP(3) O_{39}			1.60192	1.59295	1.62030	1.61647	1.63119	1.61698	–	–	–	1.63866	
			–	–	–	–	–	–				–	
σ^*N_1–H_5	0.13728	0.12237	0.08178	0.08470	0.06068	0.05814	0.05007	0.05751	0.03966	0.03635	0.03731	0.03386	0.03620
	–	–	–	–	–	–	–	–	–	–	–	–	–
σ^*O_{39}–H_5	–	–	–	–	–	–	–	–	–	–	–	–	–
	0.04018	0.04078	0.04291	0.04238	0.04511	0.04427	0.04633	0.04541	0.04777	0.04658	0.04815	0.04684	0.04830
σ^*O_{25}–H_{32}	0.09582	–	0.07408	–	0.06018	–	0.05230	–	0.04362	–	0.04151	–	0.04047
	0.03283	–	0.03349	–	0.03396	–	0.03420	–	0.03458	–	0.03463	–	0.03466
σ^*S_{25}–H_{32}	–	0.06329	–	0.05028	–	0.03675	–	0.03636	–	0.02092	–	0.01888	–
	–	0.02135	–	0.02146	–	0.02204	–	0.02236	–	0.02268	–	0.02273	–
Resonance energies													
$LP_1(O_{10}) \rightarrow \sigma^*(N_1$–$H_5)$	8.63	7.78	5.61	5.79	4.29	4.11	3.54	4.07	2.76	2.52	2.58	2.32	2.49
	–	–	–	–	–	–	–	–	–	–	–	–	–
$LP_2(O_{10}) \rightarrow \sigma^*(N_1$–$H_5)$	52.01	43.19	23.39	24.46	15.0	14.15	11.39	13.93	8.17	7.23	7.49	6.53	7.17
	–	–	–	–	–	–	–	–	–	–	–	–	–
$LP_1(O_{10}) \rightarrow \sigma^*(O_{39}$–$H_5)$	–	–	–	–	–	–	–	–	–	–	–	–	–
	6.14	3.45	7.38	7.58	8.16	8.38	8.56	8.84	–	9.26	9.11	9.37	9.14

Table 3 continued

Compound	1a	2a	1a	2a	1a	2a	1a	2a	1a	2a	1a	2a	1a
	1b	2b	1b	2b	1b	2b	1b	2b	1b	2b	1b	2b	1b
ε	1	1	2.22	2.22	4.33	4.33	7.58	7.58	24.55	24.55	46.7	46.7	78.39
$LP_2(O_{10}) \rightarrow \sigma^*(O_{39}–H_5)$	–	–	–	–	–	–	–	–	–	–	–	–	–
	3.76	6.75	4.22	3.50	4.99	4.13	5.55	4.57	–	4.99	6.31	5.02	6.36
$LP_1(N_{27}) \rightarrow \sigma^*(O39–H_5)$	–	–	–	–	–	–	–	–	–	–	–	–	–
	2.04	1.74	1.56	1.42	1.38	1.26	1.29	1.17	1.18	1.1	1.18	1.07	1.17
$LP_1(O_{38}) \rightarrow \sigma^*(O_{25}–H_{32})$	12.73	–	11.89	–	10.01	–	8.67	–	7.07	–	6.66	–	6.46
	–	–	–	–	–	–	–	–	–	–	–	–	–
$LP_2(O_{38}) \rightarrow \sigma^*(O_{25}–H_{32})$	36.21	8.45	24.34	–	17.01	–	13.55	–	10.21	–	9.47	–	9.11
	–	–	–	–	–	–	–	–	–	–	–	–	–
$LP_1(O_{38}) \rightarrow \sigma^*(S_{25}–H_{32})$	–	6.47	–	4.96	–	3.0	–	2.95	–	0.38	–	0.64	–
	–	–	–	–	–	–	–	–	–	–	–	–	–
$LP_2(O_{38}) \rightarrow \sigma^*(S_{25}–H_{32})$	–	6.60	–	4.76	–	2.85	–	2.80	–	0.94	–	0.74	–
	–	–	–	–	–	–	–	–	–	–	–	–	–
$LP_1(O_{39}) \rightarrow \sigma^*(O_{46}–H_{48})$	7.84	8.49	12.17	10.93	14.88	13.59	16.66	13.66	18.76	15.55	19.29	15.45	19.52
	–	–	–	–	–	–	–	–	–	–	–	–	–
$LP_2(O_{39}) \rightarrow \sigma^*(O_{46}–H_{48})$	–	0.86	1.04	–	1.64	–	2.55	–	4.65	3.25	5.39	4.61	5.83
	–	–	–	–	–	–	–	–	–	–	–	–	–
$LP_3(O_{39}) \rightarrow \sigma^*(O_{46}–H_{48})$	–	–	13.06	12.51	17.14	18.39	20.59	18.56	26.37	27.92	28.43	29.56	29.38
	–	–	–	–	–	–	–	–	–	–	–	–	–

His-Ser-Gln (0.272080 and 0.146458 Å vs. 0.402369 and 0.190850 Å). Both sequences also have the similar RMSD and Rg fluctuation ranges during the simulation period. These facts indicate that the side chain mutation and replacement of sulfur with oxygen leads to reduction of molecular packing and fluctuations.

On the other hand, the average structural parameters and RMS fluctuations of the backbone dihedral angles of the studied sequences were evaluated from the 40 ns MD trajectory (see Table 2). It can be seen, that the rotameric states of the involved residues are, in most cases, freer to change during the simulation in His-Ser-Gln than in His-Cys-Gln. Since histidine residue has the large imidazol ring as side chain. Hence, RMS fluctuations of involved dihedral angles (φ_{1-9}, φ_{6-18}, φ_{6-19}) are minimal in both interested sequences. According to the table data, the related dihedral angles to backbone-side chain atoms are freer to change during the simulation than those in the backbone- backbone.

As we know, the CHARMM force field uses flexible bond, angle bends, dihedral bond torsions, improper dihedral bond torsions, Lennard/Jones terms for non-bonded interactions and 1–4 interactions, electrostatic interactions between partial charges located at the atoms and Urey/Bradley (UB) terms for 1–3 interactions. The general form of the potential is given by:

$$U(R) = \sum_{\text{bonds}} K_b(b - b_0)^2 + \sum_{\text{angles}} K_\theta(\theta - \theta_0)^2 + \sum_{\text{dihedrals}} K_\chi(1 + Cos(n\chi - \delta)) + \sum_{\text{impropers}} K_\varphi(\varphi - \varphi_0)^2 + \sum_{\text{nonbond}} \left(\varepsilon_{ij} \left[\left(\frac{R_{\min,ij}}{r_{ij}} \right)^{12} - 2 \left(\frac{R_{\min,ij}}{r_{ij}} \right)^{6} \right] + \frac{q_i q_j}{\varepsilon_i r_{ij}} \right) + \sum_{UB} K_{UB}(S - S_0)^2 \quad (2)$$

The comparison of the obtained structures from quantum mechanics optimizations in different media and the average structure from MD simulations in water box represent that the explicit water molecules cause a decrease in bond length, bond and torsional angles strains of the studied structures, which can increase the stability of the investigated structures. These results are in good agreement with the experimental results on the protein structure (Havel 1996). The RMS fluctuations of the backbone atoms in the interested sequences were also evaluated from the 40 ns MD trajectory for each atom individually (see Tables 4, 5). By averaging these RMS fluctuations over all backbone atoms belonging to a given residue, we got a measure of the flexibility of each residue. The fluctuations of the backbone atoms together with the hydrogen-bonding pattern provide a consistent description of the structural flexibility of the studied sequences. According to the obtained results, it is evident that due to formation of strong hydrogen bonds between the positively charged ammonium group and the negatively charged carboxylat group with simulated water molecules, middle residues are more flexible than the terminal residues in both sequences. In addition, RMS fluctuations over all backbone atoms belonging to the residues of His-Ser-Gln sequence are higher than those of His-Cys-Gln sequence. On the other hands, the study of hydrogen bonding pattern of the interested sequences represents that average occupancy and life time of hydrogen

Table 4 RMS fluctuations (RMSF) of the backbone atoms for each residue containing His-Ser-Gln and His-Cys-Gln sequences

RMSF (A°)						
	N	C	C α	C β	O	S
His-Ser-Gln						
His	4.9491	4.4760	4.7744	5.1979	4.803	–
Ser	5.1198	4.9417	5.0590	5.1979	5.2717	–
					6.1919	
Gln	4.9491	4.4760	4.7744	5.1979	4.7719	–
					4.5605	
His-Cys-Gln						
His	4.1054	3.5323	3.8508	4.4642	3.6277	–
Cys	5.0366	4.4951	4.6191	4.4642	4.5231	4.3310
Gln	4.1054	3.5323	3.8508	4.4642	4.5022	–
					3.9911	

bonds in His-Cys-Gln sequence are higher than those in His-Ser-Gln sequence. However, it can be concluded that large values of average occupancy and lifetime of hydrogen bonds are in general associated with small average fluctuations.

4 Conclusion

The above reported quantum mechanics calculations and molecular dynamics simulations provide a reasonable picture from structural and energetic for one of the considered active site sequences of *B. cepacia* lipase,His86-Ser87-Gln88, and its mutated form, His86-Cys87-Gln88.effectively, the results show that:

- The relative stability of zwitterionic and neutral configurations depends on the solvent structure and its dielectric constant. The obtained results show that increase in the energy variance between neutral and zwitterionic forms results from increase in solvent dielectric constant.
- The NBO analyses represent that the energy variance and relative stability of zwitterionic and neutral structures are controlled by $\sigma_{*\ \mathrm{N1–H5}}$ and $\sigma_{*\ \mathrm{O39–H5}}$ antibonding pair orbital occupancies.
- The comparison of the obtained structures from quantum mechanics optimizations in different media and the average structure from MD simulations show that the explicit water molecules cause a decrease in bond length, torsional and bond angles strains of the studied structures, which can increase the stability of the investigated structures.
- These simulations also indicated that side chain mutation and replacement of sulfur with oxygen leads to reduction of the molecular flexibility and packing.

Table 5 Lifetime average and occupancy of donor/acceptor of hydrogen bonds (HB) from MD simulations for His-Ser-Gln and His-Cys-Gln sequences

	His-Ser-Gln		His-Cys-Gln	
	Lifetime (ps)	Occupancy	Lifetime (ps)	Occupancy
His-Ser-Gln				
HB donor/acceptor				
H3 →OH2 48	20	–	–	–
H3 →OH2 170	–		280	–
H4 → OH2 28	40	–	–	–
H4 → OH2 59	–	–	60	–
H4 → OH2 80	10	–	–	–
H4 → OH2 200	10	–	–	–
H5→ OH2 6	10	–	–	–
H5 → OH2 203	10	–	20	–
H11→ OH2 191	130	–	–	
H22→ OH2 117	–	–	10	–
H25→ OH2 64	–	–	10	–
H25→ OH2 184	50	–	–	–
H33→ OH2 58	140	–	–	–
H33→ OH2 46	10	–	–	–
H33→ OH2 129	–	–	40	–
H33→ OH2 139	10	–	–	–
HE21→ OH2 112	10	–	–	–
H47→ OH2 20	–	–	60	–
H48→ OH2 150	–	–	10	–
Atomic species				
H3	47.8540	1.0815	49.2729	1.1013
H4	43.5497	1.1073	47.597	1.1042
H5	47.6211	1.0810	48.5510	1.1058
H22	31.5015	0.5088	22.8860	0.9635
H25	32.8655	0.9778	11.7444	0.6480
H11	96.9750	0.9698	30.2714	0.5298
H33	40.6640	0.7502	39.0260	0.8615
H47	15.0401	0.5633	14.6144	0.5780
848	17.8593	0.7238	17.5719	0.7635

– RMS fluctuations over all backbone atoms belonging to the residues of His-Ser-Gln sequence are higher than those of His-Cys-Gln sequence. On the other hand, the study of hydrogen bonding pattern demonstrates that average occupancy and lifetime of hydrogen bonds in His-Cys-Gln sequence are higher than those in His-Ser-Gln sequence. However, it can be concluded that large values of average occupancy and lifetime of hydrogen bonds are in general associated with small average fluctuations.

References

Becke AD (1993) Density functional thermochemistry. III. The role of exact exchange. J Chem Phys 98:5648–5652. doi:10.1063/1.464913

Berendsen HJC, Postma JPM, Van Gunsteren WF, Dinola A, Haak JR (1984) Molecular dynamics with coupling to an external bath. J Chem Phys 81:3684–3690. doi:10.1063/1.448118

Brooks BR, Bruccoleri RE, Olafson BD, States DJ, Swaminathan S, Karplus M (1983) CHARMM: a program for macromolecular energy, minimization, and dynamics calculations. J Comp Chem 4:187–217. doi:10.1002/jcc.540040211

Brünger AT, Karplus M (1988) Polar hydrogen positions in proteins: Empirical energy placement and neutron diffraction comparison. Proteins Struct Funct Bioinformatics 4:148–156. doi:10.1002/prot.340040208

Creighton TE (1993) Proteins: structures and molecular properties. W.H. Freeman, New York

Faber K (1997) Biotransformations in organic chemistry, 3rd edn. Springer, Berlin

Foresman JB, Frisch Æ (1996) Exploring chemistry with electronic structure methods, 2nd edn. Gaussian Inc, Pittsburgh, PA

Frisch MJ, Trucks GW, Schlegel HB, Pople JA et al (1998) Gaussian. Inc, Pittsburgh, PA

Glendening ED, Reed AE, Carpenter JE, Weinhold F (1988) NBO Version 3.1

Grochulski P, Li YG, Schrag JD, Bouthillier F, Smith P, Harrison D, Rubin B, Cygler M (1993) Insights into interfacial activation from an open structure of Candida rugosa lipase. J Mol Catal B: Enzym 268:12843–12847. doi:10.2210/pdb1crl/pdb

Guex N, Peitsch MC (1997) SWISS-MODEL and the Swiss-PdbViewer: an environment for comparative protein modeling. Electrophoresis 18:2714–2723. doi:10.1002/elps.1150181505

Guieysse D, Salagnad C, Monsan P, Remaud-Simeon M, Tran V (2003) Towards a novel explanation of *Pseudomonas cepacia* lipase enantioselectivity via molecular modelling of the enantiomer trajectory into the active site. Tetrahedron Asym 14:1807–1817. doi:10.1016/S0957-4166(03)00374-4

Han D, Rhee JS (1986) Characteristics of lipase-catalyzed hydrolysis of olive oil in AOT-isooctane reversed micelles. Biotechnol Bioeng 28:1250–1255. doi:10.1002/bit.260280817

Havel HA (1996) Spectroscopic methods for determining protein structure in solution. VCH, New York

Honig B, Sharp K, Yang AS (1993) Macroscopic models of aqueous solutions: biological and chemical applications. J Phys Chem 97:1101–1109. doi:10.1021/j100108a002

Jacoby SLS, Kowalik KS, Pizzo JT (1972) Iterative methods for nonlinear optimization problems. Prentice-Hall, Englewood Cliffs, NJ

Jalkanen KJ, Suhai S (1996) N-acetyl-L-alanine N′-methylamide: a density functional analysis of the vibrational absorption and vibrational circular dichroism spectra. Chem Phys 208:81–116. doi:10.1016/0301-0104(96)00042-0

Jorgensen WL, Chandrasekhar J, Madura JD (1983) Comparison of simple potential functions for simulating liquid water. J Chem Phys 79:926–936. doi:10.1063/1.445869

Kim KK, Song HK, Shin DH, Hwang KY, Suh SW (1997) The crystal structure of a triacylglycerol lipase from *Pseudomonas cepacia* reveals a highly open conformation in the absence of a bound inhibitor. Structure 5:173–185. doi:10.1016/S0969-2126(97)00177-9

Lang DA, Mannesse MLM, De Haas GH, Verheij HM, Dijkstra BW (1998) Structural basis of the chiral selectivity of *Pseudomonas cepacia* lipase. Eur J Biochem 254:333–340. doi:10.1046/j.1432-1327.1998.2540333.x

Lee C, Yang W, Parr RG (1988) Development of the Colle-Salvetti correlation-energy formula into a functional of the electron density. Phys Rev B 37:785–789. doi:10.1103/PhysRevB.37.785

Ljubovic E, Sunjic V (2000) Comparative study of conformational effects on stereoselective lipase catalysed acetylation of sec hydroxy groups in diastereomeric 14-membered lactones and their acyclic analogs. Tetrahedron Lett 41:9135–9138. doi:10.1016/S0040-4039(00)01634-8

Lui′c M, Tomi′c S, Leščić I, Ljubovi′c E, Sepac D, Sunji′c V, Vitale LJ, Saenger W, Koji′c-Prodi′c B (2001) Complex of *Burkholderia cepacia* lipase with transition state analogue of 1-phenoxy-2-acetoxybutane. Eur J Biochem 268:3964–3973. doi:10.1046/j.1432-1327.2001.02303.x

MacKerell ADJ, Bashford D, Bellott M et al (1998) All-atom empirical potential for molecular modeling and dynamics studies of proteins. J Phys Chem B 102:3586–3616. doi:10.1021/jp973084f

Pugazhenthi G, Kumar A (2004) Enzyme membrane reactor for hydrolysis of olive oil using lipase immobilized on modified PMMA composite membrane. J Membr Sci 228:187–197. doi:10.1016/j.memsci.2003.10.007

Reed AE, Curtiss LA, Weinhold F (1988) Intermolecular interactions from a natural bond orbital, donor-acceptor viewpoint. Chem Rev 88:899–926. doi:10.1021/cr00088a005

Schmid RD, Verger R (1998) Lipases: interfacial enzymes with attractive applications. Angew Chem Int Ed Engl 37:1608–1633. doi:10.1002/(SICI)1521-3773(19980703)37:12<1608:AID-ANIE1608>3.0.CO; 2-V

Tafi A, van Almsick A, Corelli F, Crusco M, Laumen KE, Schneider MP, Botta M (2000) Computer simulations of enantioselective ester hydrolyses catalyzed by *Pseudomonas cepacia* lipase. J Org Chem 65:3659–3665. doi:10.1021/jo9919198

Tafi A, Manetti F, Botta M, Casati S, Santaniello E (2004) A drop of enantioselectivity in the *Pseudomonas cepacia* lipase-catalyzed ester hydrolysis is influenced by the chain length of the fatty acid. Tetrahedron Asym 15:2345–2350. doi:10.1016/j.tetasy.2004.06.010

Tajkhorshid E, Paizs B, Suhai S (1997) Conformational effects on the proton affinity of the Schiff base in bacteriorhodopsin: a density functional study. J Phys Chem B 101:8021–8028. doi:10.1021/jp971283t

Tomasi J, Persico M (1994) Molecular interactions in solution: an overview of methods based on continuous distributions of the solvent. Chem Rev 94:2027–2094. doi:10.1002/chin.199508316

Tomić S, Kojić-Prodić B (2002) A quantitative model for predicting enzyme enantioselectivity: application to *Burkholderia cepacia* lipase and 3-(aryloxy)-1, 2-propanediol derivatives. J Mol Graph Model 21:241–252. doi:10.1016/S1093-3263(02)00148-1

Tuomi WV, Kazlauskas RJ (1999) Molecular basis for enantioselectivity of lipase from *Pseudomonas cepacia* toward primary alcohols. Modeling, kinetics, and chemical modification of Tyr29 to increase or decrease enantioselectivity. J Org Chem 64:2638–2647. doi: 10.1021/jo981783y

Wiberg KB (1965) A Scheme for strain energy minimization. Application to the cycloalkanes. J Am Chem Soc 87:1070–1078. doi:10.1021/ja01083a024